Performance of a Non-Local van der Waals Density Functional on the Dissociation of H_2 on Metal Surfaces

Mark Wijzenbroek, David M. Klein, Bauke Smits, Mark F. Somers, and Geert-Jan Kroes[*]

Leiden Institute of Chemistry, Gorlaeus Laboratories, Leiden University, P.O. Box 9502, 2300 RA, Leiden, The Netherlands

E-mail: g.j.kroes@chem.leidenuniv.nl

Abstract

Van der Waals functionals have recently been applied to obtain a potential energy surface to describe the dissociation of H_2 on Ru(0001), where an improvement was found for computed reaction probabilities compared to experiment, which could not be achieved with the use of other exchange–correlation functionals. It is, however, not yet clear to what extent van der Waals functionals give a better description of other molecule–metal surface systems. In this study, the optPBE-vdW-DF functional is compared to the SRP48 functional, which was originally fitted to describe the dissociation of H_2 on Cu(111), in terms of the resulting potential energy surfaces and results of quasi-classical dynamics calculations and their agreement with experiment for different H_2–metal surface systems. It is found that overall the optPBE-vdW-DF functional yields potential energy surfaces which are very similar to potential energy surfaces computed with the SRP48 functional. In dynamics calculations the optPBE-vdW-DF functional gives a slightly better description of molecular beam experiments. Also a different dependence of reaction on the rotational quantum number J is found, which is in better agreement with experimental data for H_2 dissociation on Cu(111). The vibrational efficacy is found to be relatively insensitive to which of the two functionals is chosen.

1 Introduction

To perform accurate calculations on molecule–surface reactions, it is important to have an accurate potential energy surface (PES). It is, however, not clear which precise electronic structure method should be used to compute such a PES in order to obtain a desirable accuracy. In practice, due to limitations in computational power, one is limited to density functional theory (DFT)[1,2] using approximate exchange–correlation functionals. These functionals are usually taken to be generalized gradient approximation (GGA)[3–8] level functionals due to the larger computational expense of higher methods such as meta-generalized

2

gradient approximation (meta-GGA)[9–11] level functionals, and hybrid functionals,[12] which introduce Hartree-Fock exchange into the functional. Additionally, because for such systems often only dynamical properties such as reaction probabilities are known from experiments, and no or little knowledge is available from higher level electronic structure methods, it is often necessary to perform dynamics calculations.[13,14] This further makes such investigations computationally challenging, as either a high dimensional potential energy surface is needed, or dynamics needs to be performed based on energies and forces computed directly on the DFT level in 'ab initio molecular dynamics' (AIMD) calculations.

One particular example of such reactions is the dissociation of H_2 on metal surfaces. This particular example is a useful benchmark system for electronic structure methods, for several reasons. First of all, a large amount of experimental data is available for such systems. Additionally, these systems have also been well studied in theoretical calculations using various electronic structure and dynamics methods (see for instance references 13–23).

Second, in general molecule–surface systems are rather complex because, apart from the degrees of freedom of the molecule, in principle also degrees of freedom from the surface should be included, such as phonons and electron–hole pair excitations.[15,24,25] It is however expected for hydrogen dissociation on metal surfaces that the effects associated with these degrees of freedom are rather limited. For H_2 dissociation on metal surfaces the neglect of electron–hole pair excitations and surface motion seems to be a good approximation. For H_2 dissociation on Pt(111), it has been argued[16] that electron–hole pair excitations should not play an important role in such processes. For H_2 dissociation on Cu(111),[26,27] Cu(110)[28] and Ru(0001)[22] non-adiabatic effects have been taken into account in dynamical calculations using electronic friction. In these calculations no large non-adiabatic effects were found, which suggests that for H_2/metal systems the Born-Oppenheimer approximation works well. Furthermore, for activated dissociation systems energy exchange with phonons is expected to be a small effect[29,30] due to the large mass mismatch between the H_2 molecule and a metal surface atom. The validity of the neglect of surface motion and surface temperature has been

recently tested for H_2 dissociation on Cu(111), using ab initio molecular dynamics (AIMD) calculations,[21] in which the surface atoms were allowed to move. Additionally, calculations have been performed on the same system using a static corrugation model (SCM),[31] in which energy exchange with the surface is not possible, but the displacement of surface atoms and thermal expansion of the crystal lattice are taken into account. In particular, in both studies, a good agreement with ideal static surface calculations was found for H_2 dissociation on a low temperature Cu(111) surface ($T_s = 120$ K).

Finally, because hydrogen is a small and simple molecule, if the surface degrees of freedom are neglected, the PES of the reaction is relatively simple (6-dimensional) and it becomes feasible to accurately map out the PES. Additionally, symmetry is often present in the systems of interest and thus can often be applied in the construction of the PES, as is often done in for example the corrugation reducing procedure (CRP).[32,33] The application of symmetry can often reduce the computational costs for PESs for H_2 dissociation on ideal low-index surfaces considerably. Hydrogen/metal surface systems thus are useful for benchmarking the performance of electronic structure methods for molecule–surface reactions.[25]

Recently it has been shown for hydrogen dissociation on Ru(0001), which is a system with low barriers to reaction, that a functional containing vdW-DF[34] or vdW-DF2[35] correlation was needed to obtain a good agreement with experimental data and that other functionals did not give a proper 'width' of the reaction probability as a function of incidence energy.[23] It is however not yet clear to what extent vdW-DF-like functionals improve or worsen agreement for other systems, such as systems with a high barrier to reaction like H_2 dissociation on Cu(111) or Cu(100), or other systems with low barriers to reaction such as H_2 dissociation on Pt(111).

One of the problems of DFT for molecule–surface reactions is that computed barrier heights are often not in agreement with experiments and can differ wildly for different functionals.[18,23] It is known that for barriers of gas-phase reactions with GGA level functionals mean absolute errors are obtained which are at best 4 kcal/mol.[36–38] Recently fitted func-

tionals on the meta-GGA level have been proposed claiming mean absolute errors of about 2 kcal/mol.[38–40] It is however not clear how such functionals would perform for molecule–surface reactions as such systems have not been considered for the fitting set of these functionals.

To address the problem of accuracy in DFT, Díaz et al.[18] proposed an implementation of the 'specific reaction parameter' (SRP) approach[41] in which the exchange–correlation functional is adapted to the system at hand by optimising α in

$$E_{xc} = \alpha E_{xc}^1 + (1 - \alpha)E_{xc}^2, \tag{1}$$

where E_{xc}^1 and E_{xc}^2 are two 'standard' (i.e., GGA level) exchange–correlation functionals, of which one generally tends to provide barriers which are too low, while the other generally provides barriers which are too high. Standard exchange–correlation functionals used for molecule–surface reactions are the PW91[6] (or the similar PBE[7]) and RPBE[8] functionals. The optimisation is done in such a way that an important experiment which provides information about the barrier height is well described. As a result, one hopes that the barrier heights for the system are well described and that other observables that have not been fitted are better described for the system considered. The downside of such a procedure however is that it gives only limited predictive power, as for each specific system of interest in principle at least one experiment is needed in order to construct such a functional, which then is specific to one particular system and the quality of the description thus relies on the quality of the experiment to which the functional was fitted. Note however that the functional which was fitted for H_2 dissociation on Cu(111)[18] could also give a reasonable description of experimental data of H_2 dissociation on Cu(100),[42] suggesting that an exchange–correlation functional which works well for one system may also work well for a sufficiently similar system.

In the present study an SRP approach is not taken. Instead, in order to investigate to what extent current exchange–correlation functionals can describe H_2/metal surface systems,

and to what extent van der Waals effects are needed for a description of such systems, the performance of functionals for not one but several H_2/metal systems is considered. The H_2/Cu(111), H_2/Cu(100), H_2/Pt(111) and H_2/Ru(0001) systems are considered, because relatively well characterised experimental data is available for these systems. Two functionals are considered, one with a non-local van der Waals correction to the correlation functional and one without. For the non-corrected functional SRP48[21] is taken, as this functional gives a good agreement with experiments for H_2/Cu(111).

Over the past years, the inclusion of van der Waals effects in DFT has gathered a large interest, in particular for the interaction of molecules with surfaces.[43–47] Many methods to incorporate van der Waals effects in DFT have been developed, including the vdW-DF method by Dion et al.,[34] the DFT-D3 method by Grimme *et al.*[48] and the PBE+vdW method by Tkatchenko and Scheffler.[49] For a full overview, the reader is referred to recent review papers, such as refs. 44 or 45. In the vdW-DF method non-local correlation is used in an exchange–correlation functional instead of standard (semi-)local correlation. Several revisions of this method have been published, including revisions of the vdW-DF correlation functional such as vdW-DF2,[35] but also other exchange functionals such as optB88 and optPBE,[50] optB86b,[51] C09[52] and LV-PW86r,[53] which are intended to be used with the vdW-DF correlation functional. Recently, it has been shown for adsorption of benzene on transition metal surfaces that the optB88-vdW-DF and optPBE-vdW-DF functionals yield good adsorption energies, whereas the original vdW-DF and vdW-DF2 exchange–correlation functionals yield adsorption energies that are smaller than the experimental values.[54–56] For H_2 dissociation on Ru(0001) it was found that the vdW-DF and vdW-DF2 exchange–correlation functionals yield barriers for reaction that are too high.[23] For these reasons, here the optPBE-vdW-DF functional is chosen as the vdW-corrected functional to be tested.

In section 2 the methods used are explained, beginning with the dynamical model in section 2.1. The construction of the potential energy surfaces needed for the calculations is explained in section 2.2, the computation of observables in section 2.3 and the computational

details are given in section 2.4. The results are given in section 3, beginning with several properties and differences of the computed potential energy surfaces (PESs) in 3.1. Molecular beam sticking results are shown in section 3.2 and state-resolved reaction probabilities and rotational quadrupole alignment parameters are considered in section 3.3. Effects of changing the exchange functional and correlation functional separately are discussed in section 3.4. Finally, the conclusions are given in section 4.
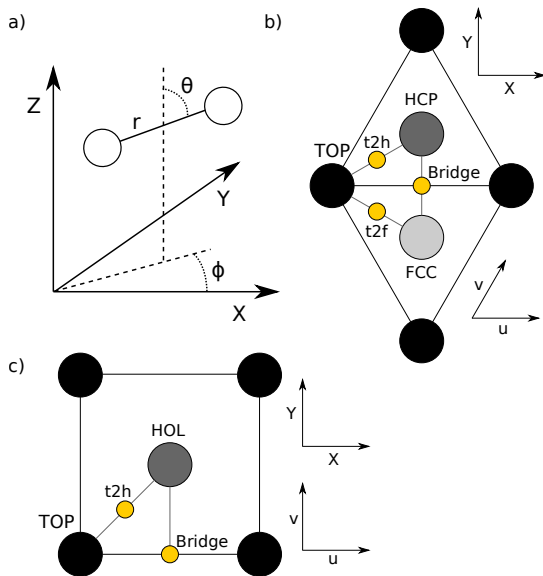
2 Theory

2.1 Dynamical model

Figure 1: (a) The center of mass coordinate system used for the description of the H_2 molecule. (b) The surface unit cell and the sites considered for the Cu(111), Pt(111) and Ru(0001) surfaces. (c) The surface unit cell and the sites considered for the Cu(100) surface. In both (b) and (c), the origin of the coordinate system ($X=u=0$, $Y=v=0$, $Z=0$) is at a top layer atom (top site). In (b), the fcc site is above a third layer atom for Cu(111) and Pt(111), but for Ru(0001) no surface atom is present at this site.

In all calculations the Born-Oppenheimer Static Surface (BOSS) model is used. In the BOSS model, first of all, the Born-Oppenheimer approximation[57] is used. Second, the surface atoms are taken to be fixed at their ideal lattice positions. As a result, only the 6 degrees of

freedom of the H_2 molecule are taken into account in the dynamical model. In figure 1(a), the coordinate system used is shown, in figure 1(b) the surface unit cell for the Cu(111), Pt(111) and Ru(0001) systems, and in figure 1(c) the surface unit cell for the Cu(100) system.

Quasi-classical dynamics calculations are performed in favour of quantum dynamics calculations for computational simplicity. For activated H_2 and, in particular, D_2 dissociation on metal surfaces, this is in general a good approximation, as shown for H_2 dissociation on Cu(111),[18,58,59] Cu(100),[60] Ru(0001)[23] and Pt(111),[61] i.e., for all systems considered here. In the dynamics calculations the Hamilton equations of motion are solved using the extrapolation method by Bulirsch and Stoer.[62] The initial conditions of the H_2 molecules are selected using standard Monte Carlo methods. In order to obtain m_J resolved reaction probabilities, the initial angular momentum of the molecule is fixed by $L = \sqrt{J(J+1)}\hbar$ and the orientation is chosen with the constraint $\cos\vartheta_L = m_J/\sqrt{J(J+1)}$, where ϑ_L is the angle between the angular momentum vector and the surface normal. To obtain accurate statistics, for each set of incidence conditions at least 10^4 trajectories were computed. The H_2 molecule is initially placed beyond the point where the PES no longer depends on Z ($Z > 6.5$ Å). The molecule is considered to have dissociated when $r > 2.25$ Å, and the molecule is considered to have scattered when $Z > 6.5$ Å with the momentum vector pointing away from the surface.

2.2   Construction of potential energy surfaces

Full 6-dimensional PESs were constructed from self-consistent DFT calculations using the optPBE-vdW-DF[50] and SRP48[21] functionals. The SRP48 functional contains a linear combination of 48% RPBE exchange[8] and 52% PBE exchange[7] together with PBE correlation.[7] The optPBE-vdW-DF functional combines an optimized PBE-like exchange functional (optPBE[50]) with vdW-DF correlation.[34]

In the interpolation of the PESs the corrugation reducing procedure (CRP)[32,33] is used. In the CRP, the PES is written as

$$V^{6D}(\vec{r}) = I^{6D}(\vec{r}) + \sum_{i}^{2} V_i^{3D}(\vec{r}_i), \tag{2}$$

in which V^{6D} is the full 6D PES of the H_2/surface system, $\vec{r}$ the vector of coordinates of the H_2 molecule with respect to the surface, I^{6D} the so-called 6D interpolation function of the H_2/surface system, which is defined by equation 2, V_i^{3D} the 3-dimensional (3D) PES of the H/surface system and $\vec{r}_i$ the vector of coordinates of the ith H atom with respect to the surface. The 3D atom–surface PES is then written as

$$V_i^{3D}(\vec{r}_i) = I_i^{3D}(\vec{r}_i) + \sum_{j}^{N} V^{1D}(R_{ij}), \tag{3}$$

in which I_i^{3D} is the 3D interpolation function describing the H/surface system, which is defined by equation 3, N the number of surface atoms taken into account in the summation, V^{1D} a 1-dimensional (1D) function mimicking the interaction of a hydrogen atom with a single surface atom and R_{ij} the distance between hydrogen atom i and surface atom j.

The idea behind the CRP is to interpolate I^{6D} instead of V^{6D}, as I^{6D} is much less corrugated in the u, v, θ and ϕ degrees of freedom than V^{6D} is.[32] The (u, v) coordinate system is a coordinate system in which the surface lattice vectors are taken as unit vectors. For H_2 dissociation on Cu(111), Pt(111) and Ru(0001) the skewing angle of this coordinate system thus is 60°, while for H_2 dissociation on Cu(100) the skewing angle is 90° as for the Cartesian coordinate system (also see figure 1(b) and (c)). The interpolation over u, v, θ and ϕ is done using symmetry adapted functions, in a way similar to the method used for H_2/Cu(100) by Olsen et al.[33] The interpolation procedure used for C_{3v} potentials (for the H_2/Cu(111), Pt(111) and Ru(0001) systems) is the same as used in reference 23 for H_2/Ru(0001) (C_{3v} symmetry). The interpolation for H_2/Cu(100) (C_{4v} symmetry) is detailed below.

For the interpolation of I^{6D} for potentials with C_{4v} symmetry, 16 configurations (u, v, θ, ϕ) are used, spread over 4 different sites (u, v). These sites are also shown in figure 1(c).

Table 1: Configurations used in the interpolation of the H_2/Cu(100) PESs. The sites listed here correspond to the sites listed in table 2, and are also shown graphically in figure 1(c).

Site	θ	ϕ
Top	0	
Top	90	0, 45
t2h	0	
t2h	45	45, 135, 225
t2h	90	45, 135
Hollow	0	
Hollow	90	0, 45
Bridge	0	
Bridge	90	0, 45, 90

The configurations used are shown in table 1. The interpolation is done in several steps. First, for every configuration, the interpolation is performed over the r and Z degrees of freedom. For this interpolation a 14×14 ($r \times Z$) grid is used employing a 2-dimensional cubic spline interpolation, where $r_{\min} = 0.4$ Å, $r_{\max} = 2.3$ Å, $Z_{\min} = 0.25$ Å and $Z_{\max} = 4$ Å. Then, for every site (u, v) the interpolation is performed over the θ and ϕ degrees of freedom using symmetry adapted sine and cosine functions. Finally, an interpolation over u and v is performed, for which again symmetry adapted sine and cosine functions are used.

In order to represent interactions that are rather long-ranged in the potential, the potential is switched between $Z = 3.4$ Å and 4.0 Å from the full 6D potential to a 2D gas-phase potential only dependent on r and Z, because far away from the surface the corrugation is small. This gas phase potential is represented by

$$V^{2D}(r, Z) = V^{\text{ext}}(Z) + V^{\text{gas}}(r), \tag{4}$$

where V^{ext} is a function describing the dependence of the PES on Z beyond $Z = 4$ Å and V^{gas} is the interaction at $Z = Z_{\max}$. $Z_{\max}$ is taken to be 6.5 Å.

For the interpolation of I^{3D} 6 sites in (u, v) are used for the potentials with C_{4v} symmetry, which are listed in table 2. The sites b2h and t2b correspond to the sites in between bridge and hollow, and top and bridge, respectively. For each site, 57 points are taken in Z, with

Table 2: Sites used in the interpolation of the H/Cu(100) PES.

Site	u	v
Top	0	0
t2h	1/4	1/4
Hollow	1/2	1/2
b2h	1/2	1/4
Bridge	1/2	0
t2b	1/4	0

$Z_{\min} = -1.06$ Å and $Z_{\max} = 5.6$ Å. The reference function V^{1D} is taken to be the interaction of the H atom above the top site, as used in previous studies.[32]

2.3 Computation of observables

2.3.1 Degeneracy averaged reaction probabilities

Degeneracy averaged initial state-resolved reaction probabilities $P_{\deg}$ are computed by

$$P_{\deg}(v, J) = \sum_{m_J=0}^{J} \left(2 - \delta_{m_J 0}\right) P_r(v, J, m_J)/(2J + 1), \tag{5}$$

in which P_r is the completely initial state-resolved reaction probability, δ the Kronecker delta and v, J and m_J are the initial vibrational, rotational and magnetic rotational quantum numbers of the H_2 molecule, respectively.

2.3.2 Rotational quadrupole alignment parameter

The rotational quadrupole alignment parameter is used to establish whether there is an orientational preference for reaction. The rotational quadrupole alignment parameter $A_0^{(2)}$ is defined by

$$A_0^{(2)} = \left\langle 3\cos^2 \vartheta_L - 1 \right\rangle, \tag{6}$$

in which ϑ_L is the angle between the angular momentum vector and the surface normal. It can be computed by[63]

$$A_0^{(2)}(v, J) = \frac{\sum_{m_J} P_r(v, J, m_J) \left(\frac{3m_J^2}{J(J+1)} - 1 \right)}{\sum_{m_J} P_r(v, J, m_J)}. \tag{7}$$

2.3.3 Molecular beam sticking probabilities

The molecular beams used in experiments to measure sticking probabilities do generally not consist of molecules in a single state with one specific amount of energy. The experimental distributions should therefore be taken into account when comparing theoretical results to experimental data. The experimental conditions are taken into account in two steps. First, the initial state-resolved reaction probabilities are Boltzmann averaged over the rovibrational states populated in the molecular beam. Second, the experimental spread of incidence energies is taken into account. The first point is addressed by

$$R_{\mathrm{mono}}(E_i; T_n) = \sum_{v, J} F_B(v, J; T_n) P_{\mathrm{deg}}(E_i, v, J). \tag{8}$$

R_{mono} is the mono-energetic reaction probability averaged over all states present in the molecular beam with a nozzle temperature T_n. The reaction probability of each state is weighed with the Boltzmann factor

$$F_B(v, J; T_n) = \frac{w(J) F(v, J; T_n)}{\displaystyle\sum_{v', J' \equiv J \ (\mathrm{mod}\ 2)} F(v', J'; T_n)}, \tag{9}$$

in which

$$F(v, J; T_n) = (2J + 1) \exp\left(-E_{\mathrm{vib}}(v, J)/(k_B T_n)\right)$$
$$\cdot \exp\left(-E_{\mathrm{rot}}(v, J)/(0.8 \cdot k_B T_n)\right). \tag{10}$$

In equation 9 the summation runs only over the values of J' that have the same parity as J. E_{vib} and E_{rot} are the vibrational and rotational energy, respectively, of the (v, J) state and k_B is the Boltzmann constant. In these equations, it is assumed that the rotational temperature of the molecules in the beam is lower than the nozzle temperature $(T_{\text{rot}} = 0.8 \cdot T_n)$.[64] It is also assumed that the fractions of ortho- and para-H_2 and D_2 are equivalent to the high temperature limit, given by $w(J)$. This is usually the case in experiments, as the gas cylinder is stored at room temperature and conversion of ortho- and para-hydrogen does not happen on the time scale of the experiment. For H_2, $w(J)$ is equal to 1/4 for even J and 3/4 for odd J. For D_2, $w(J)$ is equal to 2/3 for even J and 1/3 for odd J.

The mono-energetic reaction probability is then averaged over the translational energy distribution by[58]

$$R_{\text{beam}} = \frac{\int_0^\infty f(v_i; T_n) R_{\text{mono}}(E_i; T_n) dv_i}{\int_0^\infty f(v_i; T_n) dv_i}. \tag{11}$$

In this equation f is the flux weighted velocity distribution, which is given by[65,66]

$$f(v_i; T_n) dv_i = C v_i^3 \exp\left[-(v_i - v_0)^2/\alpha^2\right] dv_i. \tag{12}$$

In equation 12 C is a constant, v_i the velocity of the molecule, v_0 is the stream velocity and α is a parameter describing the width of the velocity distribution.

2.3.4 Vibrational efficacy

The vibrational efficacy is a measure of how 'efficiently' vibrational energy can be used to promote reaction relative to (normal) translational energy.[67,68] It can be computed by

$$\chi_v(J) = \frac{E_0(v=0, J) - E_0(v=1, J)}{E_{\text{vib}}(v=1, J) - E_{\text{vib}}(v=0, J)} = \frac{\Delta E_0}{\Delta E_{\text{vib}}}, \tag{13}$$

in which $E_{\text{vib}}(v, J)$ is the vibrational energy corresponding to a particular state of the gas-phase molecule and $E_0(v, J)$ is the energy for which $P_r(E_0; v, j) = P_{r,0}(v, J)$, where $P_{r,0}(v, J)$

is a particular value of the reaction probability. This reaction probability is commonly taken to be half the saturation value of the reaction probability.[67] In calculations often the convention is used that $P_{r,0}(v = 0, J) = P_{r,0}(v = 1, J)$. This convention may differ from the one often used by experimentalists if the saturation values differ for $v = 0$ and $v = 1$, or because a $P_{r,0}$ is selected that does not correspond to half the saturation value for any v.

2.4   Computational details

For the electronic structure calculations version 5.2.12 of the VASP[69–72] software package was used. For calculations with the SRP48 functional, the standard[73] VASP ultrasoft pseudopotentials[74] were used. For the optPBE-vdW-DF functional, the standard[72] projector augmented wave (PAW)[75] potentials were used. VASP evaluates the non-local vdW-DF correlation functional within the scheme of Román-Pérez and Soler.[76]

For the computation of the PESs, a $9\times9\times1$ Γ-centered k-point mesh was used with a plane wave cutoff of 400 eV, except for the H_2/Ru(0001) PESs where a $8\times8\times1$ mesh was used with a plane wave cutoff of 350 eV. For H_2 dissociation on Cu(100) and Cu(111), a 4 layer slab was used, while for H_2 dissociation on Ru(0001) and Pt(111) a 5 layer slab was used, which is consistent with previous calculations[16,18,23,42] on these systems. In all cases a 2×2 supercell was considered with a 13 Å vacuum between different images of the slab. Fermi smearing with a width of 0.1 eV was used to speed up convergence of the DFT calculations. The convergence with respect to the plane wave cutoff and k-point sampling was tested for H_2/Cu(111) and H_2/Pt(111) at three different geometries close or at the barrier and is expected to be well within 10 meV of the fully converged value.

Table 3: Barrier heights (E), positions (r, Z) and energetic corrugation (ξ, in eV) for SRP48 and optPBE-vdW-DF PESs for H_2 dissociation on Cu(111), Cu(100), Ru(0001) and Pt(111) above three different sites. For all geometries, $\theta = 90°$. On the HCP and hollow sites, $\phi = 0°$. Also see figure 1(b) and 1(c) and the definitions given in the text.

|		SRP48			optPBE-vdW-DF		
		E (eV)	r (Å)	Z (Å)	E (eV)	r (Å)	Z (Å)
Cu(111)	BtH	0.636	1.030	1.172	0.712	1.053	1.165
	TtB	0.887	1.396	1.394	0.915	1.382	1.396
	HCP	1.047	1.539	1.269	1.070	1.427	1.271
	ξ	0.411			0.358		
Cu(100)	BtH	0.742	1.239	0.992	0.822	1.237	0.996
	HOL	0.836	1.099	1.031	0.896	1.112	1.050
	TtB	0.867	1.432	1.379	0.883	1.413	1.383
	ξ	0.125			0.074		
Ru(0001)	TtB	0.066	0.757	2.650	-0.013	0.755	2.662
	BtH	0.281	0.789	1.997	0.219	0.793	1.934
	HCP	0.398	0.812	1.869	0.361	0.835	1.762
	ξ	0.332			0.374		
Pt(111)	TtB	0.102	0.767	2.292	0.034	0.774	2.152
	HCP	0.490	0.847	1.669	0.506	0.874	1.602
	BtH	0.492	0.837	1.602	0.530	0.862	1.506
	ξ	0.390			0.496		
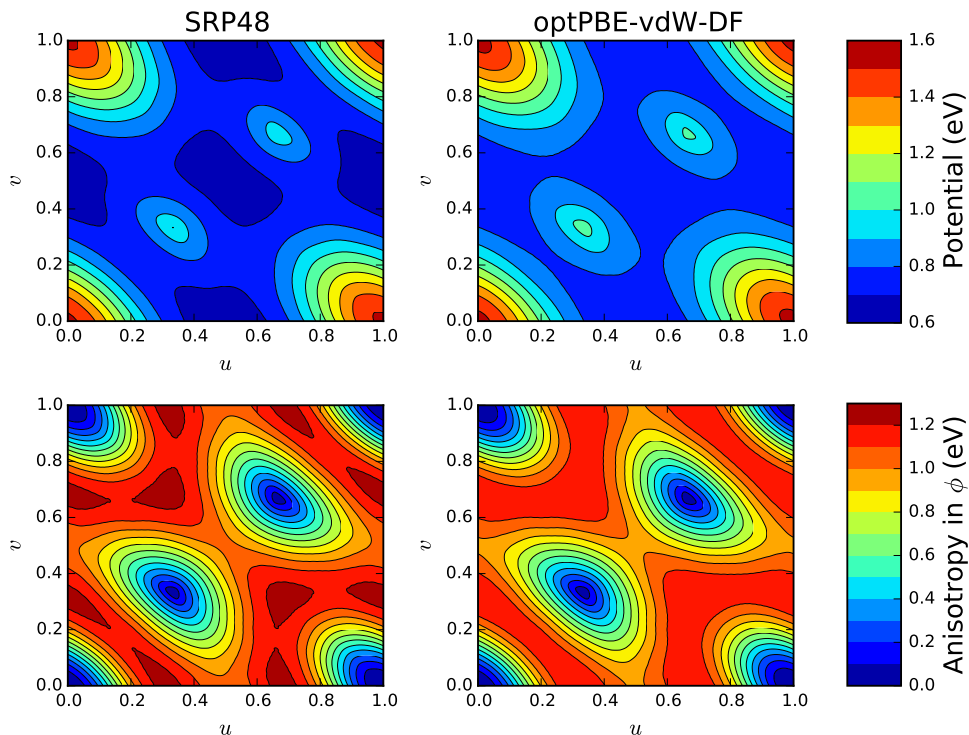
Figure 2: (u, v) dependence of the potential energy surfaces for H_2 dissociation on Cu(111), for $r = 1.2$ Å, $Z = 1.2$ Å and $\theta = 90°$. Top panels: full potential with ϕ optimized. Bottom panels: anisotropy in ϕ, as explained in the text.

3 Results and discussion

3.1 Potential energy surfaces and barrier heights

In table 3 barrier heights are given for three high symmetry dissociation paths for the computed potential energy surfaces, together with the distance of the H_2 molecule to the surface (Z) and the distance between the two H atoms (r) at the transition state. For the H_2/Cu(111) and H_2/Cu(100) systems, both functionals predict the lowest barrier to be for bridge-to-hollow (BtH) dissociation, consistent with previous calculations.[18,42] For these systems the energetic corrugation (denoted in table 3 by ξ, here defined as the difference between the highest and lowest investigated barrier) is smaller for the optPBE-vdW-DF functional than for the SRP48 functional. For the H_2/Ru(0001) and H_2/Pt(111) systems, both func-

tionals predict the lowest barrier to be for top-to-bridge (TtB) dissociation, which is also consistent with previous calculations.[16,20,23,77] For these systems the optPBE-vdW-DF functional yields a larger energetic corrugation than the SRP48 functional. Compared to the SRP48 barrier heights, for the H_2/Cu(111) and H_2/Cu(100) systems the optPBE-vdW-DF functional generally predicts larger barrier heights, whereas the optPBE-vdW-DF barrier heights for H_2/Ru(0001) are generally smaller. For H_2/Pt(111), the optPBE-vdW-DF barrier height is smaller for TtB dissociation, but larger for HCP and BtH dissociation.

The barrier positions for the two PESs are similar for the H_2/Cu(111) and H_2/Cu(100) systems, but less so for the H_2/Ru(0001) and H_2/Pt(111) systems, where the barriers for optPBE-vdW-DF are mostly closer to the surface than for SRP48. For H_2/Ru(0001), in a study where a large number of functionals were considered, it was found for the TtB barrier that functionals containing vdW-DF correlation predict a barrier closer to the surface than functionals containing another type of correlation, e.g. PBE correlation as used in the SRP48 functional, for a similar barrier height.[23] The present results for Ru(0001), but also for Pt(111), are in agreement with this.

In figure 2 the (u, v) dependence of the SRP48 and optPBE-vdW-DF PESs for H_2 dissociation on Cu(111) is shown, together with the anisotropy in ϕ at the same points, for a point ($r = 1.2$ Å, $Z = 1.2$ Å) close to the barrier geometry with $\theta = 90°$. The anisotropy in ϕ is here defined as the difference between the highest and lowest potential encountered while rotating the molecule around $360°$ over ϕ for $\theta = 90°$. The potential energy shown in the top panels is the minimum potential energy encountered during this rotation over ϕ.

The anisotropy of the two potentials close to the barrier geometry is remarkably similar, with the anisotropy for optPBE-vdW-DF being slightly lower than the anisotropy for SRP48. The remarkable similarity between the SRP48 and optPBE-vdW-DF PESs for both the full potential, minimized over ϕ, and the anisotropy in ϕ, as well as the barrier positions shown in table 3, suggests that also dynamical observables that are dependent on more detailed properties of the PES, such as the anisotropy or the corrugation of the PES should be

reasonably similar, except for a small shift or broadening due to the different barrier heights. Similar plots for the other systems considered show similar behaviour in the sense that the anisotropy of the SRP48 and optPBE-vdW-DF PESs is at least qualitatively similar.
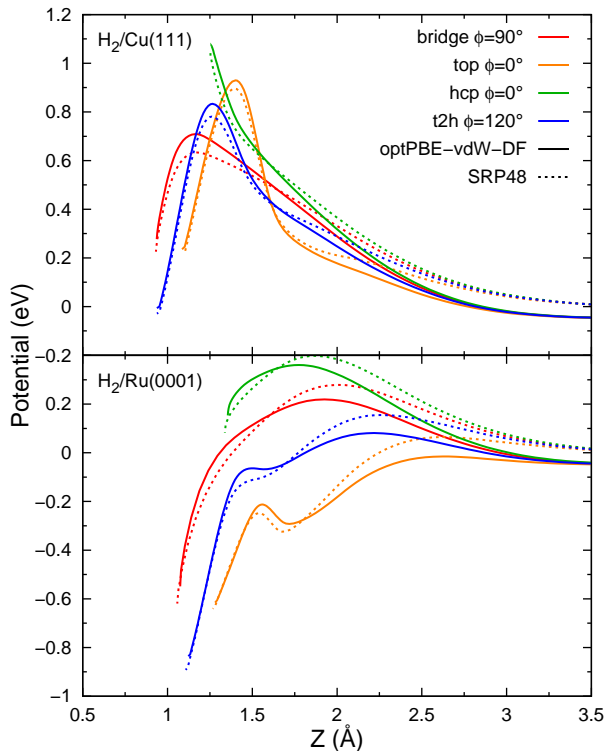

Figure 3: Reaction paths based on NEB calculations on a spline interpolation of computed 2-dimensional PES cuts for the H_2/Cu(111) and H_2/Ru(0001) systems, for 4 different dissociation geometries. A potential of 0 eV corresponds to the gas-phase minimum. Results for optPBE-vdW-DF are indicated by solid lines, while results for SRP48 are indicated by dotted lines.

Minimum energy paths were computed with the nudged elastic band method applied to 2D cuts through the interpolated PES for H_2 dissociation on Cu(111) and Ru(0001) for 4 different dissociation pathways. These pathways are shown in figure 3. Several features of the PES are apparent in this figure. First of all, far away from the surface, near $Z = 3.5$ Å, the optPBE-vdW-DF potential is lower than the SRP48 potential. This is a result of the van der Waals attraction, which leads to a well in the PES. This well is present in the optPBE-vdW-DF PESs, but not in the SRP48 PESs, as (semi-)local functionals such as SRP48 cannot describe van der Waals effects.[45] Beyond this well, moving the molecule

18

closer to the surface, the PES for both functionals qualitatively changes in the same way: the ordering of the potential for different reaction paths is the same for both surfaces.

There are, however, some more subtle differences which seem to be relevant. First of all, for H_2 dissociation on Cu(111), the optPBE-vdW-DF potential rises more quickly when the molecule is moved toward the surface than for the SRP48 potential. This causes the optPBE-vdW-DF and SRP48 potentials to cross one another at about $Z = 1.6$ Å. Second, for H_2 dissociation on Ru(0001), similar effects occur although the effects seem smaller here. In this case a similar crossing occurs as for Cu(111), but here the crossing occurs after the SRP48 transition state, at about $Z = 1.6 - 1.8$ Å, similar to the crossing for Cu(111). In the optPBE-vdW-DF PES, the Z dependence of the potential for H_2/Ru(0001) is also somewhat stronger than in the SRP48 PES, although this effect seems to be smaller than for H_2 dissociation on Cu(111). The barriers for H_2 dissociation on Ru(0001) are generally closer to the surface for optPBE-vdW-DF than for SRP48. H_2/Cu(100) behaves similarly to H_2/Cu(111), while H_2/Pt(111) behaves similarly to H_2/Ru(0001).

It is clear that such effects should be present if a functional with a van der Waals correction is used which, additionally, gives the same or nearly the same description of the barrier height as the non-vdW functional, as is the case here. The interaction present in the regular, non-vdW corrected functional approximately starts at a value of Z which corresponds to the bottom of the van der Waals well. In order to obtain the same barrier height and position with the vdW functional that the non-vdW functional would yield (the effective barrier from this point to reaction has gone up by the well depth), this non-vdW interaction in the vdW corrected functional either has to start earlier (larger Z) or has to be stronger (as in, yields a stronger Z dependence of the potential). As shown in figure 3, the non-vdW interaction does not seem to start earlier for optPBE-vdW-DF than for SRP48 (an extrapolation of the SRP48 curves to the bottom of the well in figure 3 suggests the interaction should then start at $Z \approx 3.5$ Å). As this is not the case, the Z dependence of the potential should be stronger. A proper van der Waals corrected functional for such systems is therefore expected to yield

a steeper Z dependence than a non-vdW corrected functional would.

By considering these effects for early and late barriers it is possible to explain the differences between SRP48 and optPBE-vdW-DF barriers in table 3, as well as make more general predictions for differences between van der Waals and standard GGA functionals. Due to the steeper Z dependence of the PES, for late barriers, which occur beyond the crossing point ($Z < 1.6$ Å), the barrier will in general be increased by going from SRP48 to optPBE-vdW-DF. For systems containing only late barriers, such as the highly activated H_2/Cu(111) and H_2/Cu(100) here, all barrier heights will therefore in general increase. For early barriers, which occur before the crossing point ($Z > 1.8$ Å), the barrier will in general be lowered and occur at a smaller value of Z for the optPBE-vdW-DF functional. The results in table 3 are mostly in agreement with this. It is however still unclear precisely why for H_2 dissociation on Ru(0001) the optPBE-vdW-DF BtH and HCP barriers occur at smaller values of Z compared to SRP48. It should be noted that for H_2 dissociation on Ru(0001) it was previously found that there is a trend between the barrier height and position, in the sense that higher barriers generally occur closer to the surface.[23,77] For systems containing early barriers such as H_2/Pt(111) and H_2/Ru(0001) however, in general both earlier and later barriers will be present, and for these systems the later barriers therefore increase slightly compared to the earlier barriers, yielding an increased energetic corrugation. It should be noted that, in principle, these arguments can be extended to other pairs of well performing functionals and systems as well, provided that one knows where the crossing point for the two functionals occurs, which is determined by the steepness of the potential in Z and the depth of the physisorption well.

3.2   Molecular beam sticking

In figure 4 sticking probabilities are shown for D_2 dissociation on Cu(111), H_2 dissociation on Cu(100) and D_2 dissociation on Ru(0001), and the initial state-resolved reaction probability is shown for ($v = 0, J = 0$) D_2 dissociation on Pt(111), for the optPBE-vdW-DF and SRP48
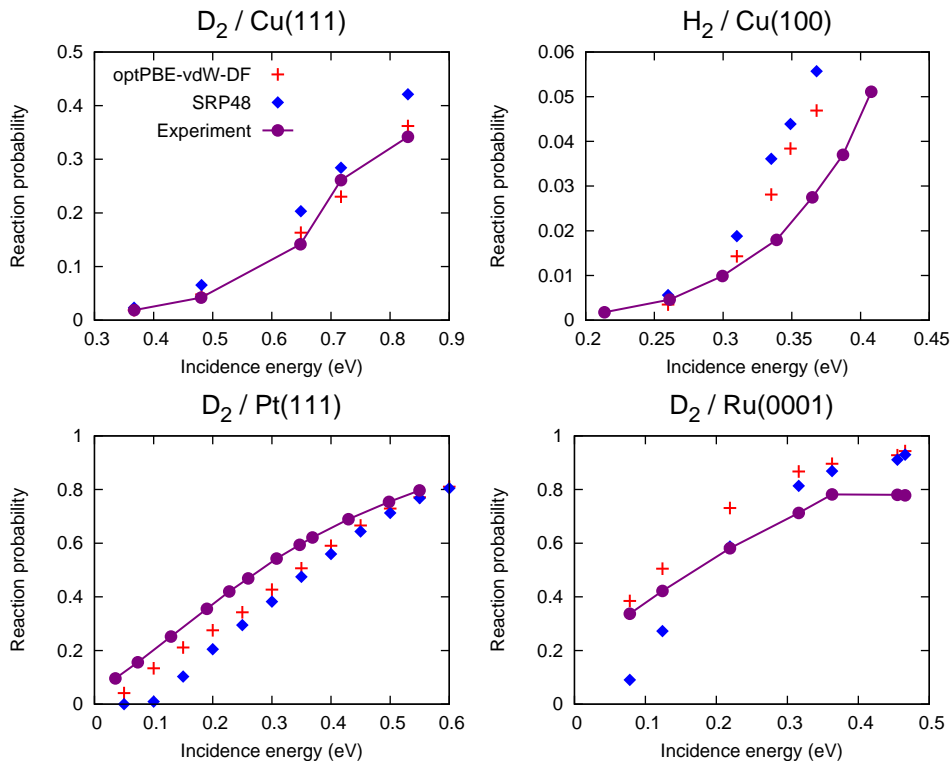
Figure 4: Molecular beam simulations for the optPBE-vdW-DF and SRP48 functionals, applied to the four systems considered in this study. Beam parameters used for the Cu(111) and Cu(100) calculations were taken from Díaz et al.[18] Beam parameters used for the Ru(0001) calculations were taken from Wijzenbroek et al.[23] For the Pt(111) surface the ($v = 0$, $J = 0$) reaction probability is shown as no beam parameters are known. Experimental data for Cu(111) by Michelsen et al.,[67] for Cu(100) by Anger et al.,[78] for Pt(111) by Luntz et al.[79] and Ru(0001) by Groot et al.[80]

functionals. A comparison is made with available experimental data.[67,78–80] As expected, for D_2 dissociation on Cu(111) the SRP48 reaction probability is in good agreement with experiment. This is not surprising because this functional was constructed[18,21] to reproduce this particular molecular beam experiment. The optPBE-vdW-DF functional also performs well, giving somewhat lower reaction probabilities in line with the higher barriers present in the PES (see table 3). For H_2 dissociation on Cu(100) the same holds. The agreement for the SRP48 functional is similar to that found in previous calculations with a similar functional,[42] and the agreement for the optPBE-vdW-DF functional is again somewhat better due to the higher barriers to dissociation given by this functional. For D_2 dissociation on Pt(111) and Ru(0001), however, the optPBE-vdW-DF functional gives higher reaction probabilities than the SRP48 functional. For D_2 dissociation on Pt(111), the agreement is better for the optPBE-vdW-DF functional than for the SRP48 functional. The optPBE-vdW-DF reaction probability rises less steeply with increasing incidence energy than the SRP48 reaction probability. Such a 'broadening' effect resulting from the use of exchange–correlation functionals containing vdW-DF correlation was also previously found for hydrogen dissociation on Ru(0001).[23] Finally, for D_2 dissociation on Ru(0001), the SRP48 functional gives a reaction probability curve which is too narrow, which was also found in previous calculations with a similar functional.[20] The optPBE-vdW-DF functional gives a somewhat better width for the reaction probability curve and better agreement with experiment. Overall, for the systems considered here, the optPBE-vdW-DF functional tends to outperform the SRP48 functional.

3.3 State-resolved reaction probability and rotational quadrupole alignment

In figure 5 the reaction probability for $(v = 0, J = 0)$ and $(v = 1, J = 0)$ D_2 dissociating on Cu(111) is shown for the SRP48 and optPBE-vdW-DF functionals. Despite the difference in energetic corrugation (for SRP48 $\xi = 0.411$ eV, while for optPBE-vdW-DF $\xi = 0.358$ eV),
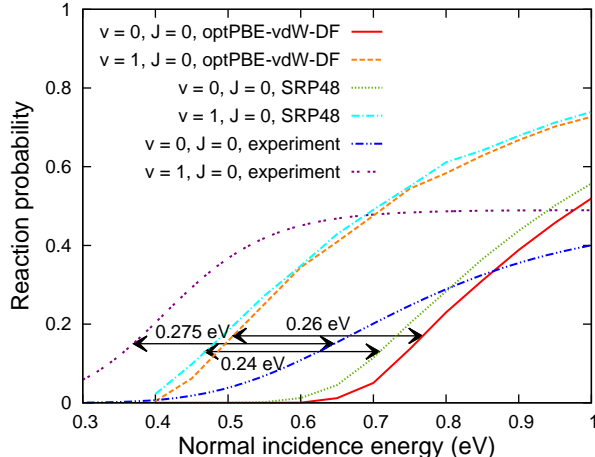
22

Figure 5: Reaction probability as a function of normal incidence energy for $(v = 0, J = 0)$ D_2 and $(v = 1, J = 0)$ D_2 dissociating on Cu(111) for the SRP48 and optPBE-vdW-DF functionals. ΔE_0 at a reaction probability of 15% are indicated. Experimental data for T_s = 925 K by Michelsen et al.,[67] reanalysed by Nattino et al.[81]

for neither $(v = 0, J = 0)$ nor $(v = 1, J = 0)$ D_2 noticeable differences are found between the slopes of the reaction probability curves obtained with the two functionals, which contrasts with the large difference found for H_2 dissociation on Ru(0001).[23] The $(v = 0)$ and $(v = 1)$ curves have a similar shape and slope for each functional, in disagreement with the results of the analysis of experiments, which show large differences between the slopes of $(v = 0)$ and $(v = 1)$ curves.[67,81] Note, however, that the effect of surface temperature is not taken into account in the calculations reported here, and it is known from experiments that this should cause a broadening of the reaction probability curves, which should be prominent at the experimental T_s (925 K).[82,83]

Table 4: Vibrational efficacy for $(v = 0 \rightarrow 1)$ D_2 dissociating on Cu(111).

Method	Vibrational efficacy
SRP48	0.65
optPBE-vdW-DF	0.71
Re-analysis[81] ($P_{r,0} = 0.05$)	0.62
Re-analysis[81] ($P_{r,0} = 0.15$)	0.74
Re-analysis[81] ($P_{r,0} = 0.25$)	0.88

The use of the optPBE-vdW-DF functional leads to a slightly higher value of the vi-

brational efficacy ($\chi_v = 0.71$) than the use of the SRP48 functional ($\chi_v = 0.65$) (see table 4). This reflects the slightly larger shift of the ($v = 1$) reaction probability curve relative to the ($v = 0$) curve for the optPBE-vdW-DF functional (0.26 eV) than observed for the SRP48 functional (0.24 eV, see equation 13). These numbers can be compared to the value of χ_v that can be obtained from a recent re-analysis[81] of the original experimental data.[67] This experimental value depends on the value selected for $P_{r,0}$ used to define E_0 in equation 13 (see section 2.3.4) because the shapes of the reaction probability curves for ($v = 1$) and ($v = 0$) extracted from experiment differ: for $P_{r,0} = 0.15$, $\chi_v = 0.74$ is obtained, and for $P_{r,0} = 0.05$, $\chi_v = 0.62$ (see table 4). To which theoretical value of χ_v the experimental value should be compared is not so straightforward. The experimental fits could be argued to be the most accurate where the time of flight intensity is highest. For ($v = 0$, $J = 0$) this is at a reaction probability of about 0.1. On the other hand, the reaction probability at the so-called effective barrier height in the old experimental fits was 0.135 and 0.25, for $v = 0$ and $v = 1$, respectively. To a good approximation, at the corresponding collision energy the reaction probability does not vary with T_s.[82,83] A useful compromise therefore seems to be to evaluate the vibrational efficacy for a reaction probability of about 0.15. As it is not fully clear which reaction probability should be considered, the vibrational efficacy is shown for several values of the reaction probability in table 4. On the basis of these values, no preference for SRP48 or optPBE-vdW-DF can be found from the calculated χ_v, as both functionals perform equally well. Finally, note that the experimental value for $D_2/Cu(111)$ was originally reported to be χ_v 0.54,[67] but this was based on a different definition of the vibrational efficacy, in which different values for $P_{r,0}$ are used for $v = 0$ and 1.

In figure 6 the reaction probability for ($v = 0$, $J = 0, 2, 4, 6, 8$) D_2 dissociating on Cu(111) is shown for both tested functionals, also comparing to the reaction probability curves extracted from experiments.[81] The analysis of the experimental results showed that reaction first decreases with J, up to about $J = 4$, and then increases with J.[67,81] The behaviour of the optPBE-vdW-DF results is closest to this: for optPBE-vdW-DF, up to $J = 6$ no large
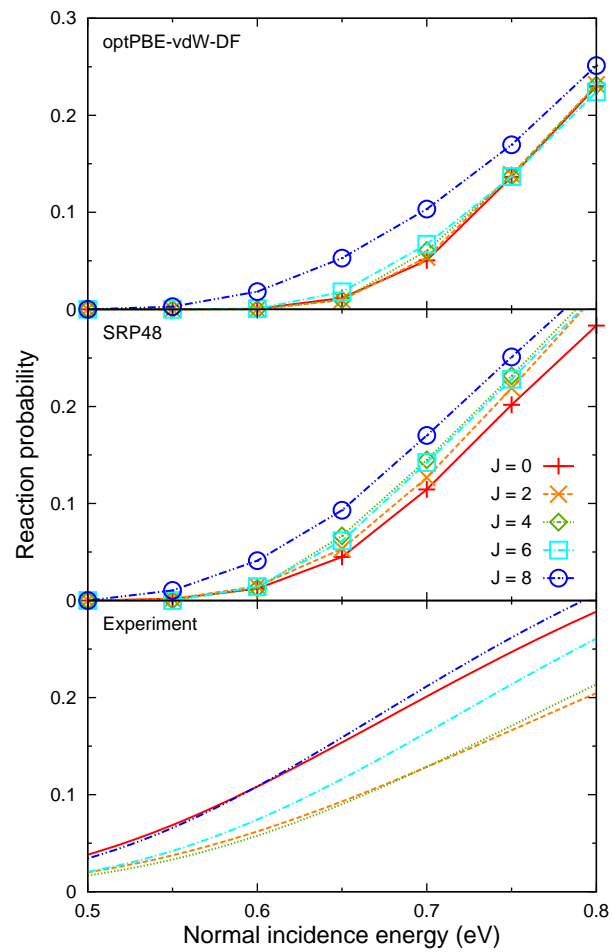
24

Figure 6: Reaction probability as a function of normal incidence energy for several rotational states of D_2 dissociating on Cu(111) for the optPBE-vdW-DF and SRP48 functionals. Fits to experimental results[67] at $T_s = 925$ K by Nattino et al.[81]

dependence of reaction on J is found, and for higher J the reaction probability increases with J. For the SRP48 functional, however, reaction actually increases up to about $J = 4$, in direct contrast to the behaviour observed in experiment. The optPBE-vdW-DF functional therefore seems to show a somewhat better performance than the SRP48 functional.
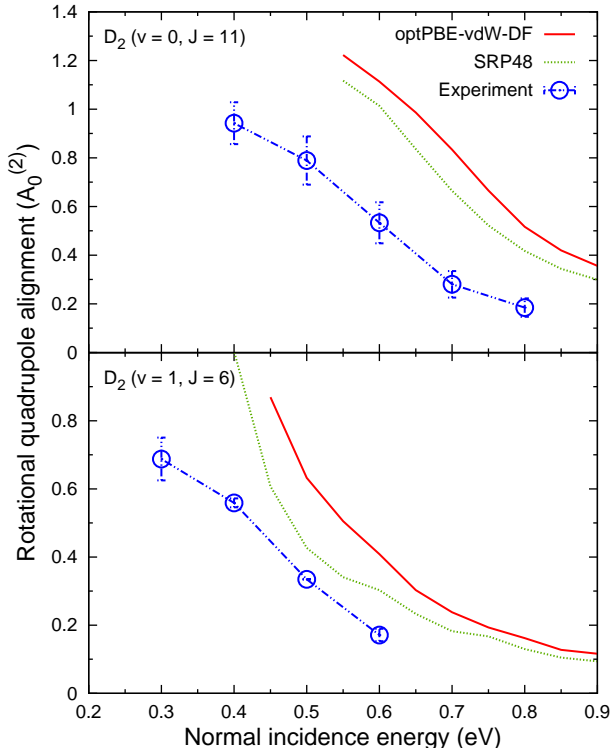

Figure 7: Rotational quadrupole alignment parameter for D_2 dissociation on Cu(111) as a function of normal incidence energy for the optPBE-vdW-DF and SRP48 functionals. Experimental results at $T_s = 925$ K by Hou et al.[84]

In figure 7 the rotational quadrupole alignment parameter $A_0^{(2)}(v, J)$ is shown for $(v = 0, J = 11)$ and $(v = 1, J = 6)$ D_2 dissociating on Cu(111) for both functionals, also comparing to experiments.[84] The $A_0^{(2)}(v, J)$ computed with SRP48 is shifted to lower energies than the one computed with optPBE-vdW-DF for both states at all energies considered, by about 0.05 eV for $(v = 0, J = 11)$ and 0.06 eV for $(v = 1, J = 6)$. The agreement of the static ideal surface theoretical results with the experimental data is not so good for either state and for either functional. However, previous work employing the SRP48 functional[21] and a similar functional[31] showed that taking into account the effect of the surface temperature

used in the experiments (925 K[84]) leads to a substantial decrease of the computed $A_0^{(2)}(v, J)$ and to much better agreement with experiment, although the computed $A_0^{(2)}(v, J)$ were still somewhat too high. Taking into account the surface temperature for the optPBE-vdW-DF functional should also lead to a decrease in the $A_0^{(2)}(v, J)$ computed with this functional, and to a better agreement with experiment. It is however not yet clear whether surface temperature has the same quantitative effect for the optPBE-vdW-DF functional, and it is therefore not yet fully clear which functional performs better for $A_0^{(2)}(v, J)$.

3.4 The effect of changing the exchange and the correlation functionals separately

In the above sections, dynamics results for two exchange–correlation (XC) functionals, i.e., the SRP48 and the optPBE-vdW-DF XC functionals, have been discussed. One might wonder whether some of the results that are obtained, such as the better performance of optPBE-vdW-DF for sticking of D_2 on Ru(0001) (figure 4) or the difference in performance of the two functionals for reproducing the $A_0^{(2)}$ measured for D_2 + Cu(111) (figure 7), is due to changing the exchange functional, the correlation functional, or both. The following can be said about this.

Table 5: **Minimum barrier height (E, in eV) and energetic corrugation (ξ, in eV), of H_2 + Cu(111) obtained with the optPBE and PBE exchange functionals combined with PBE correlation.**

Exchange functional	E (eV)	ξ (eV)
optPBE	0.460	0.416
PBE	0.484	0.406

Starting from the SRP48 functional, changing only the exchange functional amounts to using the optPBE exchange functional and the PBE correlation functional ("optPBE-PBE"). Inspection of table 5 suggests that this would yield a functional that is similar to the PBE functional: for H_2 + Cu(111), the minimum barrier height and the energetic corrugation are very similar for these functionals. However, it is known that the PBE

functional does not yield a correct description of sticking of H_2 to Ru(0001) (see figure 10 of ref. 23) because functionals with PBE correlation underestimate the energetic corrugation of the H_2 + Ru(0001) PES.[23] Specifically, with the PBE functional the sticking probability is considerably overestimated at large average collision energies, and the same would be expected to hold for the similar optPBE-PBE functional. In contrast, reasonable values of both the minimum barrier height and the energetic corrugation can be obtained by using vdW-DF correlation. In fact, using SRP48 exchange and vdW-DF correlation would be very similar to using one of the candidate SRP functionals that described sticking of H_2 and D_2 to Ru(0001) quite well[23] and even better than the optPBE-vdW-DF functional. Here, the only difference between the SRP48 and the candidate SRP functional is that the former employs 48% RPBE and 52% PBE exchange, whereas the latter uses 50% RPBE and 50% PBE exchange. In other words, the better performance of the optPBE-vdW-DF functional than that of SRP48 comes from changing the PBE to the vdW-DF correlation functional, and not from changing the SRP48 to the optPBE exchange functional.

Similarly, the good performance of the optPBE-vdW-DF functional for H_2 + Cu(111) does certainly not come only from changing the SRP48 to the optPBE exchange functional. As discussed above (see again table 5) optPBE-PBE and PBE yield very similar values of the minimum barrier height and energetic corrugation of H_2 + Cu(111). However, it is known that using the PW91 functional[6] leads to hugely overestimated sticking probabilities for H_2 + Cu(111) when comparing with experimental values.[18] The same should hold for the PBE functional, as the PBE functional was designed to reproduce PW91 energies,[7] and the PBE and PW91 barrier heights for H_2 + Cu(111) are indeed very similar.[18] Then, the use of the optPBE-PBE functional should likewise lead to hugely overestimated sticking probabilities for H_2 + Cu(111). Quantum dynamics calculations using a PW91 PES suggest that using the optPBE-PBE functional to compute $A_0^{(2)}$ values for D_2 + Cu(111) should likewise lead to incorrect results: within the static and ideal surface approximation, the use of PW91 leads to computed $A_0^{(2)}$ values that underestimate the experimental values for ($v = 1$, $J = 6$) D_2

(see figure 11 of ref. 58). Also taking into account the effect of the high surface temperature in the experiments (925 K[84]) would lead to a further decrease of the computed $A_0^{(2)}$,[21,31] and, therefore, to an even worse comparison with experiment. In other words, maintaining good agreement with experiment for H_2 + Cu(111) depends on changing not only the exchange functional, but also the correlation functional when changing the SRP48 XC functional to the optPBE-vdW-DF XC functional.

4   Conclusions and outlook

Potential energy surfaces are constructed for the dissociation of H_2 on Cu(111), Cu(100), Pt(111) and Ru(0001) from density functional theory calculations using two different exchange–correlation functionals, one with non-local vdW-DF correlation (optPBE-vdW-DF) and one with standard GGA (PBE) correlation (SRP48). To determine to what extent using the non-local vdW-DF functional improves the description of the molecule–surface interaction over the non-corrected case, the potential energy surfaces for the two functionals have been compared to one another in terms of barrier heights, anisotropy in ϕ and the corrugation in u and v. A comparison is also made between reaction probabilities and rotational quadrupole alignment parameters obtained from quasi-classical dynamics calculations and experiments, where possible.

In the analysis of the PESs in terms of barrier heights, different behaviours were found for the weakly activated H_2/Pt(111) and H_2/Ru(0001) systems on the one hand and the highly activated H_2/Cu(111) and H_2/Cu(100) systems on the other hand. For H_2 dissociation on Ru(0001) and Pt(111), the barriers are generally found to be later for the optPBE-vdW-DF PES than for the SRP48 PES, whereas for H_2 dissociation on Cu(111) and Cu(100) the barriers were approximately equally late. For H_2 dissociation on Ru(0001) and Pt(111), the energetic corrugation (difference in barrier height of the lowest and highest investigated barrier) is larger for optPBE-vdW-DF than for SRP48, whereas for H_2 dissociation on Cu(111)

and Cu(100) the opposite is found. This is explained by considering the minimum energy pathways to dissociation for several geometries. For both H_2 dissociation on Ru(0001) and Cu(111), the minimum energy pathways cross at a value of $Z \approx 1.6 - 1.8$ Å. If the barrier occurs after this crossing (closer to the surface), as for H_2 dissociation on Cu(111) and Cu(100), the barrier is generally increased because optPBE-vdW-DF shows a more steeply rising potential along the reaction path. If the barrier occurs before this crossing, as found for H_2 dissociation on Ru(0001) and Pt(111), the barrier is lowered, because the optPBE-vdW-DF functional shows a physisorption well far away from the surface for all considered surfaces, and the barrier is usually also later.

Dynamics results show that reaction probabilities obtained with the optPBE-vdW-DF functional tend to be in better overall agreement with experiments than the SRP48 functional. For both D_2 dissociation on Ru(0001) and Pt(111) the optPBE-vdW-DF sticking curve is broader (less steep increase with incidence energy) compared to the SRP48 sticking curve. The primary difference between the sticking curves for the D_2/Cu(111) and H_2/Cu(100) systems is a shift, the optPBE-vdW-DF functional showing overall less reactivity.

For D_2 dissociating on Cu(111) the J-dependence of reaction has also been investigated, as well as the vibrational efficacy and the rotational quadrupole alignment parameter. The vibrational efficacy as computed with the optPBE-vdW-DF functional is slightly higher than for SRP48. Based on this, and uncertainties in the experimental data, no preference for one of the two tested functionals can be assigned. For the J-dependence of reaction of D_2 on Cu(111), however, the optPBE-vdW-DF functional shows that reaction for low rotational states ($J < 8$) is virtually independent of the rotational state, whereas SRP48 shows reaction to increase with increasing J. As experimental data for this system shows reaction to decrease with increasing J state at first, the optPBE-vdW-DF results are in qualitatively better agreement with the experimental data. The rotational quadrupole alignment parameter for D_2 on Cu(111) is for both functionals too high compared to experiments. It should be noted

however, that the temperature of the surface was not taken into account in this study. It is known from previous studies that the temperature of the surface can greatly influence the rotational quadrupole alignment parameter. Although the known surface temperature dependence for SRP48 suggests this functional to work better, in order to determine a preference for either functional based on the rotational quadrupole alignment parameter the surface temperature dependence of both functionals should be investigated.

Overall, the optPBE-vdW-DF functional seems to yield results in better agreement with experimental data for the systems considered, especially for the molecular beam sticking probabilities and the width (steepness) of the associated reaction probability curves. It is satisfying to see that including non-local vdW-DF correlation in the exchange–correlation functional not only improves the description of weakly activated dissociation (as seen earlier for H_2/Ru(0001)[23]), but also of highly activated dissociation.

In the future, it would be of interest to also apply the optPBE-vdW-DF functional to non-activated dissociation problems, such as H_2 + Pd(111),[85,86] H_2 + Pd(100),[87,88] or H_2 + Ni(110).[88] A correct description of these systems would demonstrate the correct addition of strongly attractive chemical interactions to the van der Waals interaction in a region that is potentially even closer to the surface, which might constitute an additional challenge. We note that H_2 + Pd(111) has already been studied with functionals containing vdW-DF correlation; a problem with this system is that there is considerable uncertainty regarding the experimental sticking probability, due to experimental discrepancies.[89] The N_2 + W(110) system, in which the dissociation is also considerably affected by the presence of molecular chemisorption wells, has also recently been studied with the use of vdW functionals.[90] However, the outcome of these calculations should be somewhat uncertain, because the effect of energy transfer to the W(110) surface was not yet taken into account, while AIMD calculations suggest a large effect on the reactivity of this energy transfer.[91]

Acknowledgement

Supporting Information Available

The (u, v) dependence of the potential energy surfaces for H_2 dissociation on Cu(100), Ru(0001) and Pt(111), and reaction paths for H_2 dissociation on Cu(100) and Pt(111). This material is available free of charge via the Internet at `http://pubs.acs.org/`.

References

(1) Kohn, W.; Sham, L. J. Self-consistent equations including exchange and correlation effects. *Phys. Rev.* **1965**, *140*, A1133–A1138.

(2) Hohenberg, P.; Kohn, W. Inhomogeneous electron gas. *Phys. Rev.* **1964**, *136*, B864–B871.

(3) Langreth, D. C.; Mehl, M. J. Beyond the local-density approximation in calculations of ground-state electronic properties. *Phys. Rev. B* **1983**, *28*, 1809–1834.

(4) Becke, A. D. Density-functional exchange-energy approximation with correct asymptotic behavior. *Phys. Rev. A* **1988**, *38*, 3098–3100.

(5) Perdew, J. P. Density-functional approximation for the correlation energy of the inhomogeneous electron gas. *Phys. Rev. B* **1986**, *33*, 8822–8824.

(6) Perdew, J. P.; Chevary, J. A.; Vosko, S. H.; Jackson, K. A.; Pederson, M. R.; Singh, D. J.; Fiolhais, C. Atoms, molecules, solids, and surfaces: applications of the generalized gradient approximation for exchange and correlation. *Phys. Rev. B* **1992**, *46*, 6671–6687.

(7) Perdew, J. P.; Burke, K.; Ernzerhof, M. Generalized gradient approximation made simple. *Phys. Rev. Lett.* **1996**, *77*, 3865–3868.

(8) Hammer, B.; Hansen, L. B.; Nørskov, J. K. Improved adsorption energetics within density-functional theory using revised Perdew-Burke-Ernzerhof functionals. *Phys. Rev. B* **1999**, *59*, 7413–7421.

(9) Perdew, J. P.; Schmidt, K. Jacob's ladder of density functional approximations for the exchange-correlation energy. *AIP Conf. Proc.* **2001**, *577*, 1–20.

(10) Perdew, J. P.; Tao, J.; Staroverov, V. N.; Scuseria, G. E. Meta-generalized gradient approximation: Explanation of a realistic nonempirical density functional. *J. Chem. Phys.* **2004**, *120*, 6898–6911.

(11) Perdew, J. P.; Ruzsinszky, A.; Csonka, G. I.; Constantin, L. A.; Sun, J. Workhorse semilocal density functional for condensed matter physics and quantum chemistry. *Phys. Rev. Lett.* **2009**, *103*, 026403.

(12) Becke, A. D. Density-functional thermochemistry. III. The role of exact exchange. *J. Chem. Phys.* **1993**, *98*, 5648–5652.

(13) Kroes, G. J. Six-dimensional quantum dynamics of dissociative chemisorption of H_2 on metal surfaces. *Prog. Surf. Sci.* **1999**, *60*, 1–85.

(14) Kroes, G. J.; Somers, M. F. Six-dimensional dynamics of dissociative chemisorption of H_2 on metal surfaces. *J. Theor. Comput. Chem.* **2005**, *04*, 493–581.

(15) Groß, A. Reactions at surfaces studied by *ab initio* dynamics calculations. *Surf. Sci. Rep.* **1998**, *32*, 291–340.

(16) Nieto, P.; Pijper, E.; Barredo, D.; Laurent, G.; Olsen, R. A.; Baerends, E. J.; Kroes, G. J.; Farías, D. Reactive and nonreactive scattering of H_2 from a metal surface is electronically adiabatic. *Science* **2006**, *312*, 86–89.

(17) Pozzo, M.; Alfè, D. Hydrogen dissociation on Mg(0001) studied via quantum Monte Carlo calculations. *Phys. Rev. B* **2008**, *78*, 245313.

(18) Díaz, C.; Pijper, E.; Olsen, R. A.; Busnengo, H. F.; Auerbach, D. J.; Kroes, G. J. Chemically accurate simulation of a prototypical surface reaction: H_2 dissociation on Cu(111). *Science* **2009**, *326*, 832–834.

(19) Groß, A. *Ab initio* molecular dynamics simulations of the adsorption of H_2 on palladium surfaces. *ChemPhysChem* **2010**, *11*, 1374–1381.

(20) Nieto, P.; Farías, D.; Miranda, R.; Luppi, M.; Baerends, E. J.; Somers, M. F.; van der Niet, M. J. T. C.; Olsen, R. A.; Kroes, G. J. Diffractive and reactive scattering of H_2 from Ru(0001): experimental and theoretical study. *Phys. Chem. Chem. Phys.* **2011**, *13*, 8583–8597.

(21) Nattino, F.; Díaz, C.; Jackson, B.; Kroes, G. J. Effect of surface motion on the rotational quadrupole alignment parameter of D_2 reacting on Cu(111). *Phys. Rev. Lett.* **2012**, *108*, 236104.

(22) Füchsel, G.; Schimka, S.; Saalfrank, P. On the role of electronic friction for dissociative adsorption and scattering of hydrogen molecules at a Ru(0001) surface. *J. Phys. Chem. A* **2013**, *117*, 8761–8769.

(23) Wijzenbroek, M.; Kroes, G. J. The effect of the exchange-correlation functional on H_2 dissociation on Ru(0001). *J. Chem. Phys.* **2014**, *140*, 084702.

(24) Kroes, G. J. Frontiers in surface scattering simulations. *Science* **2008**, *321*, 794–797.

(25) Kroes, G. J. Towards chemically accurate simulation of molecule-surface reactions. *Phys. Chem. Chem. Phys.* **2012**, *14*, 14966–14981.

(26) Luntz, A. C.; Persson, M. How adiabatic is activated adsorption/associative desorption? *J. Chem. Phys.* **2005**, *123*, 074704.

(27) Muzas, A. S.; Juaristi, J. I.; Alducin, M.; Díez Muiño, R.; Kroes, G. J.; Díaz, C. Vibrational deexcitation and rotational excitation of H_2 and D_2 scattered from Cu(111): Adiabatic versus non-adiabatic dynamics. *J. Chem. Phys.* **2012**, *137*, 064707.

(28) Juaristi, J. I.; Alducin, M.; Díez Muiño, R.; Busnengo, H. F.; Salin, A. Role of electron–hole pair excitations in the dissociative adsorption of diatomic molecules on metal surfaces. *Phys. Rev. Lett.* **2008**, *100*, 116102.

(29) Busnengo, H. F.; Dong, W.; Sautet, P.; Salin, A. Surface temperature dependence of rotational excitation of H_2 scattered from Pd(111). *Phys. Rev. Lett.* **2001**, *87*, 127601.

(30) Busnengo, H. F.; Di Césare, M. A.; Dong, W.; Salin, A. Surface temperature effects in dynamic trapping mediated adsorption of light molecules on metal surfaces: H_2 on Pd(111) and Pd(110). *Phys. Rev. B* **2005**, *72*, 125411.

(31) Wijzenbroek, M.; Somers, M. F. Static surface temperature effects on the dissociation of H_2 and D_2 on Cu(111). *J. Chem. Phys.* **2012**, *137*, 054703.

(32) Busnengo, H. F.; Salin, A.; Dong, W. Representation of the 6D potential energy surface for a diatomic molecule near a solid surface. *J. Chem. Phys.* **2000**, *112*, 7641–7651.

(33) Olsen, R. A.; Busnengo, H. F.; Salin, A.; Somers, M. F.; Kroes, G. J.; Baerends, E. J. Constructing accurate potential energy surfaces for a diatomic molecule interacting with a solid surface: H_2+Pt(111) and H_2/Cu(100). *J. Chem. Phys.* **2002**, *116*, 3841–3855.

(34) Dion, M.; Rydberg, H.; Schröder, E.; Langreth, D. C.; Lundqvist, B. I. Van der Waals density functional for general geometries. *Phys. Rev. Lett.* **2004**, *92*, 246401.

(35) Lee, K.; Murray, E. D.; Kong, L.; Lundqvist, B. I.; Langreth, D. C. Higher-accuracy van der Waals density functional. *Phys. Rev. B* **2010**, *82*, 081101.

(36) Zheng, J.; Zhao, Y.; Truhlar, D. G. The DBH24/08 database and its use to assess electronic structure model chemistries for chemical reaction barrier heights. *J. Chem. Theory Comput.* **2009**, *5*, 808–821.

(37) Yang, K.; Zheng, J.; Zhao, Y.; Truhlar, D. G. Tests of the RPBE, revPBE, τ-HCTHhyb, ωB97X-D, and MOHLYP density functional approximations and 29 others against representative databases for diverse bond energies and barrier heights in catalysis. *J. Chem. Phys.* **2010**, *132*, 164117.

(38) Peverati, R.; Truhlar, D. G. Quest for a universal density functional: the accuracy of density functionals across a broad spectrum of databases in chemistry and physics. *Phil. Trans. R. Soc. A* **2014**, *372*, 20120476.

(39) Peverati, R.; Truhlar, D. G. M11-L: A local density functional that provides improved accuracy for electronic structure calculations in chemistry and physics. *J. Phys. Chem. Lett.* **2012**, *3*, 117–124.

(40) Peverati, R.; Truhlar, D. G. An improved and broadly accurate local approximation to the exchange-correlation density functional: The MN12-L functional for electronic structure calculations in chemistry and physics. *Phys. Chem. Chem. Phys.* **2012**, *14*, 13171–13174.

(41) Chuang, Y. Y.; Radhakrishnan, M. L.; Fast, P. L.; Cramer, C. J.; Truhlar, D. G. Direct dynamics for free radical kinetics in solution: solvent effect on the rate constant for the reaction of methanol with atomic hydrogen. *J. Phys. Chem. A* **1999**, *103*, 4893–4909.

(42) Sementa, L.; Wijzenbroek, M.; van Kolck, B. J.; Somers, M. F.; Al-Halabi, A.; Busnengo, H. F.; Olsen, R. A.; Kroes, G. J.; Rutkowski, M.; Thewes, C. et al. Reactive scattering of H_2 from Cu(100): comparison of dynamics calculations based on the specific reaction parameter approach to density functional theory with experiment. *J. Chem. Phys.* **2013**, *138*, 044708.

(43) Tkatchenko, A.; Romaner, L.; Hofmann, O. T.; Zojer, E.; Ambrosch-Draxl, C.; Scheffler, M. Van der Waals interactions between organic adsorbates and at organic/inorganic interfaces. *MRS Bull.* **2010**, *35*, 435–442.

(44) Grimme, S. Density functional theory with London dispersion corrections. *WIREs: Comput. Mol. Sci.* **2011**, *1*, 211–228.

(45) Klimeš, J.; Michaelides, A. Perspective: Advances and challenges in treating van der Waals dispersion forces in density functional theory. *J. Chem. Phys.* **2012**, *137*, 120901.

(46) Ramalho, J. P. P.; Gomes, J. R. B.; Illas, F. Accounting for van der Waals interactions between adsorbates and surfaces in density functional theory based calculations: selected examples. *RSC Adv.* **2013**, *3*, 13085–13100.

(47) Berland, K.; Cooper, V. R.; Lee, K.; Schröder, E.; Thonhauser, T.; Hyldgaard, P.; Lundqvist, B. I. van der Waals forces in density functional theory: a review of the vdW-DF method. *Rep. Prog. Phys.* **2015**, *78*, 066501.

(48) Grimme, S.; Antony, J.; Ehrlich, S.; Krieg, H. A consistent and accurate *ab initio* parameterization of density functional dispersion correction (DFT-D) for the 94 elements H-Pu. *J. Chem. Phys.* **2010**, *132*, 154104.

(49) Tkatchenko, A.; Scheffler, M. Accurate molecular van der Waals interactions from ground-state electron density and free-atom reference data. *Phys. Rev. Lett.* **2009**, *102*, 073005.

(50) Klimeš, J.; Bowler, D. R.; Michaelides, A. Chemical accuracy for the van der Waals density functional. *J. Phys.: Condens. Matter* **2010**, *22*, 022201.

(51) Klimeš, J.; Bowler, D. R.; Michaelides, A. Van der Waals density functionals applied to solids. *Phys. Rev. B* **2011**, *83*, 195131.

(52) Cooper, V. R. Van der Waals density functional: An appropriate exchange functional. *Phys. Rev. B* **2010**, *81*, 161104(R).

(53) Berland, K.; Hyldgaard, P. Exchange functional that tests the robustness of the plasmon description of the van der Waals density functional. *Phys. Rev. B* **2014**, *89*, 035412.

(54) Liu, W.; Carrasco, J.; Santra, B.; Michaelides, A.; Scheffler, M.; Tkatchenko, A. Benzene adsorbed on metals: concerted effect of covalency and van der Waals bonding. *Phys. Rev. B* **2012**, *86*, 245405.

(55) Yildirim, H.; Greber, T.; Kara, A. Trends in adsorption characteristics of benzene on transition metal surfaces: role of surface chemistry and van der Waals interactions. *J. Phys. Chem. C* **2013**, *117*, 20572–20583.

(56) Carrasco, J.; Liu, W.; Michaelides, A.; Tkatchenko, A. Insight into the description of van der Waals forces for benzene adsorption on transition metal (111) surfaces. *J. Chem. Phys.* **2014**, *140*, 084704.

(57) Born, M.; Oppenheimer, R. Zur Quantentheorie der Molekeln. *Ann. Phys. (Berlin)* **1927**, *389*, 457–484.

(58) Díaz, C.; Olsen, R. A.; Auerbach, D. J.; Kroes, G. J. Six-dimensional dynamics study of reactive and non reactive scattering of H_2 from Cu(111) using a chemically accurate potential energy surface. *Phys. Chem. Chem. Phys.* **2010**, *12*, 6499–6519.

(59) Mondal, A.; Wijzenbroek, M.; Bonfanti, M.; Díaz, C.; Kroes, G. J. Thermal lattice

expansion effect on reactive scattering of H_2 from Cu(111) at $T_s = 925$ K. *J. Phys. Chem. A* **2013**, *117*, 8770–8781.

(60) McCormack, D. A.; Kroes, G. J. Accuracy of trajectory methods for activated adsorption of H_2 on Cu(100). *Chem. Phys. Lett.* **1998**, *296*, 515–520.

(61) Pijper, E.; Somers, M. F.; Kroes, G. J.; Olsen, R. A.; Baerends, E. J.; Busnengo, H. F.; Salin, A.; Lemoine, D. Six-dimensional quantum dynamics of scattering of (v=0, j=0) H_2 from Pt(111): comparison to experiment and to classical dynamics results. *Chem. Phys. Lett.* **2001**, *347*, 277–284.

(62) Stoer, J.; Bulirsch, R. *Introduction to numerical analysis*; Springer: New York, 1980.

(63) Zare, R. N. *Angular momentum*; Wiley: New York, 1988.

(64) Rettner, C. T.; Michelsen, H. A.; Auerbach, D. J. Quantum-state-specific dynamics of the dissociative adsorption and associative desorption of H_2 at a Cu(111) surface. *J. Chem. Phys.* **1995**, *102*, 4625–4641.

(65) Michelsen, H. A.; Auerbach, D. J. A critical examination of data on the dissociative adsorption and associative desorption of hydrogen at copper surfaces. *J. Chem. Phys.* **1991**, *94*, 7502–7520.

(66) Auerbach, D. J. In *Atomic and molecular beam methods*; Scoles, G., Ed.; Oxford University Press: Oxford, 1988; Vol. 1; Chapter 14.

(67) Michelsen, H. A.; Rettner, C. T.; Auerbach, D. J.; Zare, R. N. Effect of rotation on the translational and vibrational energy dependence of the dissociative adsorption of D_2 on Cu(111). *J. Chem. Phys.* **1993**, *98*, 8294–8307.

(68) Díaz, C.; Olsen, R. A. A note on the vibrational efficacy in molecule–surface reactions. *J. Chem. Phys.* **2009**, *130*, 094706.

(69) Kresse, G.; Hafner, J. *Ab initio* molecular dynamics for liquid metals. *Phys. Rev. B* **1993**, *47*, 558–561.

(70) Kresse, G.; Furthmüller, J. Efficiency of *ab initio* total energy calculations for metals and semiconductors using a plane-wave basis set. *Comput. Mater. Sci.* **1996**, *6*, 15–50.

(71) Kresse, G.; Furthmüller, J. Efficient iterative schemes for *ab initio* total-energy calculations using a plane-wave basis set. *Phys. Rev. B* **1996**, *54*, 11169–11186.

(72) Kresse, G.; Joubert, D. From ultrasoft pseudopotentials to the projector augmented-wave method. *Phys. Rev. B* **1999**, *59*, 1758–1775.

(73) Kresse, G.; Hafner, J. Norm-conserving and ultrasoft pseudopotentials for first-row and transition elements. *J. Phys.: Condens. Matter* **1994**, *6*, 8245–8257.

(74) Vanderbilt, D. Soft self-consistent pseudopotentials in a generalized eigenvalue formalism. *Phys. Rev. B* **1990**, *41*, 7892–7895.

(75) Blöchl, P. E. Projector augmented-wave method. *Phys. Rev. B* **1994**, *50*, 17953–17979.

(76) Román-Pérez, G.; Soler, J. M. Efficient implementation of a van der Waals density functional: application to double-wall carbon nanotubes. *Phys. Rev. Lett.* **2009**, *103*, 096102.

(77) Luppi, M.; Olsen, R. A.; Baerends, E. J. Six-dimensional potential energy surface for H_2 at Ru(0001). *Phys. Chem. Chem. Phys.* **2006**, *8*, 688–696.

(78) Anger, G.; Winkler, A.; Rendulic, K. D. Adsorption and desorption kinetics in the systems H_2/Cu(111), H_2/Cu(110) and H_2/Cu(100). *Surf. Sci.* **1989**, *220*, 1–17.

(79) Luntz, A. C.; Brown, J. K.; Williams, M. D. Molecular beam studies of H_2 and D_2 dissociative chemisorption on Pt(111). *J. Chem. Phys.* **1990**, *93*, 5240–5246.

(80) Groot, I. M. N.; Ueta, H.; van der Niet, M. J. T. C.; Kleyn, A. W.; Juurlink, L. B. F. Supersonic molecular beam studies of dissociative adsorption of H_2 on Ru(0001). *J. Chem. Phys.* **2007**, *127*, 244701.

(81) Nattino, F.; Genova, A.; Guijt, M.; Muzas, A. S.; Díaz, C.; Auerbach, D. J.; Kroes, G. J. Dissociation and recombination of D_2 on Cu(111): *ab initio* molecular dynamics calculations and improved analysis of desorption experiments. *J. Chem. Phys.* **2014**, *141*, 124705.

(82) Michelsen, H. A.; Rettner, C. T.; Auerbach, D. J. On the influence of surface temperature on adsorption and desorption in the D_2/Cu(111) system. *Surf. Sci.* **1992**, *272*, 65–72.

(83) Murphy, M. J.; Hodgson, A. Adsorption and desorption dynamics of H_2 and D_2 on Cu(111): the role of surface temperature and evidence for corrugation of the dissociation barrier. *J. Chem. Phys.* **1998**, *108*, 4199–4211.

(84) Hou, H.; Gulding, S. J.; Rettner, C. T.; Wodtke, A. M.; Auerbach, D. J. The stereo-dynamics of a gas-surface reaction. *Science* **1997**, *277*, 80–82.

(85) Lesnik, J. Untersuchungen über Vorläuferadsorption an Übergangsmetallen und Übergangsmetallegierungen. Ph.D. thesis, Technischen Universität Graz, 2001.

(86) Beutl, M.; Lesnik, J.; Rendulic, K. D.; Hirschl, R.; Eichler, A.; Kresse, G.; Hafner, J. There is a true precursor for hydrogen adsorption after all: the system H_2/Pd(111) + subsurface V. *Chem. Phys. Lett.* **2001**, *342*, 473–478.

(87) Rettner, C. T.; Auerbach, D. J. Search for oscillations in the translational energy dependence of the dissociation of H_2 on Pd(100). *Chem. Phys. Lett.* **1996**, *253*, 236–240.

(88) Rendulic, K. D.; Anger, G.; Winkler, A. Wide range nozzle beam adsorption data for the systems H_2/nickel and H_2/Pd(100). *Surf. Sci.* **1989**, *208*, 404–424.

(89) Boereboom, J. M.; Wijzenbroek, M.; Somers, M. F.; Kroes, G. J. Towards a specific reaction parameter density functional for reactive scattering of H_2 from Pd(111). *J. Chem. Phys.* **2013**, *139*, 244707.

(90) Martin-Gondre, L.; Juaristi, J. I.; Blanco-Rey, M.; Díez Muiño, R.; Alducin, M. Influence of the van der Waals interaction in the dissociation dynamics of N_2 on W(110) from first principles. *J. Chem. Phys.* **2015**, *142*, 074704.

(91) Nattino, F.; Costanzo, F.; Kroes, G. J. N_2 dissociation on W(110): an *ab initio* molecular dynamics study on the effect of phonons. *J. Chem. Phys.* **2015**, *142*, 104702.

Graphical TOC Entry

Plot titled "D$_2$ / Cu(111)" showing Reaction probability versus Incidence energy (eV) with data series: optPBE-vdW-DF, SRP48, and Experiment.